

X-ray reflection by rough multilayer gratings: Dynamical and kinematical scattering

P. Mikulík

Laboratory of Thin Films and Nanostructures, Faculty of Science, Masaryk University, Kotlářská 2, 611 37 Brno, Czech Republic

T. Baumbach

Fraunhofer Institut Zerstörungsfreie Prüfverfahren, Krügerstrasse 22, D-01326 Dresden, Germany
and European Synchrotron Radiation Facility, Boîte Postale 220, F-38043 Grenoble Cedex, France

(Received 22 December 1997)

X-ray reflectivity by rough multilayer gratings is treated in the framework of kinematical and dynamical theories. The kinematical scattering integral is calculated without the restrictions of the Fraunhofer approximation. The dynamical theory is presented by the matrix modal eigenvalue approach. In both theories we generalize the Fresnel reflection and transmission coefficients for the case of grating diffraction. We obtain one unique formalism which permits us to compare the results of both theories directly. Furthermore, interface and sidewall roughnesses are taken into account. The dynamical approach allows us to explain the experimental results obtained from a partially etched GaAs/InP periodic multilayer grating. [S0163-1829(99)05308-4]

I. INTRODUCTION

Simple and multilayer gratings (MLG's) of mesoscopic scale have achieved scientific and practical applications in optical and electronic devices. X-ray scattering methods were successfully employed for the nondestructive characterization of such laterally patterned arrays. High-resolution x-ray diffraction is mostly employed for the investigation of epitaxial gratings. The method is simultaneously sensitive to the perfection of the grating shape and to the strain state in the layers. This is an advantage on the one hand, but in many cases it is difficult to distinguish between both structural influences on the diffraction pattern.

X-ray reflection (XRR) allows one to characterize crystalline, amorphous, and polycrystalline gratings, since it investigates the distribution of the mean electron density. Thus it is sensitive to the grating shape, and would also allow one to determine the quality of the interfaces.

Until now, theories of different levels of complexity were involved in the calculations of the reflected intensity, based on fully dynamical and simple kinematical approaches. Dynamical approaches from MLG's have been studied by different methods: (1) A *rigorous vector theory* for diffraction gratings was developed by Maystre¹ within the framework of classical optics. An integral equation from this work was used by Tolan and co-workers²⁻⁴ to calculate the x-ray scattering by a trapezoidal surface grating. (2) Two other methods are based on a *matrix formalism*: the *differential method*⁵ and the *modal method*.⁶⁻⁹ In the modal method the wave equation is transformed into a transcendental dispersion equation for the wave-vector components of the diffracted waves,^{6,7} or into an eigenvalue problem (for etched gratings,⁸ for planar mirrors modulated with a transverse acoustic wave⁹). The modal and differential methods have been compared for the calculation of multilayer grating efficiencies.⁸

The kinematical approach is equivalent to the first Born approximation.¹⁰ The scattering integral is always calculated using the Fraunhofer approximation.¹⁰⁻¹² Consequently, the amplitude of the scattered wave is proportional to the sample size, similar to conventional kinematical x-ray diffraction by small crystals. Thus the Fraunhofer approximation is re-

stricted on samples with a size smaller than the first Fresnel zone. This is in general not fulfilled by (laterally extended) multilayers.

The surface roughness of simple gratings was treated by Tolan *et al.*,⁴ averaging the Rayleigh-Mayster coefficients. A damping factor similar to the Névot-Croce factor¹³ of rough planar surfaces has been found. In order to explain the diminished efficiency of MLG's, a damping factor has been introduced phenomenologically in a dynamical matrix method.¹⁴

In the present paper we introduce interface roughness as well as defects of the grating shape directly in the theoretical framework of the kinematical and dynamical approaches, and apply them to XRR of semiconductor multilayer gratings (part I). The dynamical theory provides a rigorous but numerically expensive treatment. The kinematical theory is transparent, and supports the intuitive interpretation. That is why we develop in a following paper (part II) semidynamical approximations with the aim to be sufficiently precise *and* transparent to explain the essential experimental findings. In order to provide an effective comparison, we derived one unique formalism for all different approaches. In particular, we generalized the Fresnel coefficients of reflection and transmission by planar interfaces for the case of diffraction by multilayered gratings.

Mainly short-period MLG's (lateral grating period $d \approx 1 \mu\text{m}$) for electronic applications are concerned. We use the coplanar scattering geometry for wavelengths of about $\lambda \approx 1 \text{ \AA}$. Finally, we present experimental results for XRR by epitaxial multilayered gratings (partially etched GaAs/InP periodic multilayer gratings) and apply our theoretical models successfully to fit the experimental curves.

The paper is organized as follows. In Sec. II we introduce the common notation of the variables and of the geometrical parameters describing the multilayer grating. Sections III and IV cover two treatments: the kinematical and dynamical approaches. In both these sections we start with the reflection from perfect MLG's. Afterwards we consider real structural effects (the roughness of the horizontal interfaces, and defects of the sidewalls of the grating wires). Then we compare

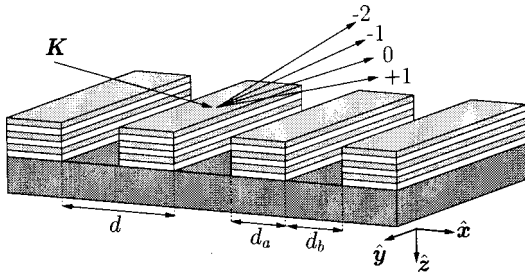


FIG. 1. Schematic representation of the reflection by a multilayer grating: the diffracted wave field above the grating consists of a fan of diffracted-reflected waves.

both theories and continue by discussing the experimental results.

II. SAMPLE SETUP AND SCATTERING POTENTIAL

The x-ray reflection pattern depends on the distribution of the refractive index n in the sample. The refractive index is related with the electrical susceptibility by $\chi = 1 - n^2$. In the present paper we will use χ instead of n in accordance with x-ray-diffraction theories. The scattering potential is for small angles of incidence and exit $V(\mathbf{r}) = -K^2\chi(\mathbf{r})$.

The considered multilayer gratings consist of $N-1$ layers deposited on a substrate (a semi-infinite layer number N) (Figs. 1 and 2). Thus there are N horizontal interfaces, the sample surface is at z_1 , and the substrate interface is at z_N . Laterally, each layer j is a periodic repetition of two wires $a^{(j)}$ and $b^{(j)}$ with the susceptibilities $\chi_a^{(j)}$ and $\chi_b^{(j)}$, respectively. The grating setup can be approximated by a layerwise rectangular profile with a layer thickness $t_j = z_{j+1} - z_j$ and widths $d_a^{(j)} = \Gamma^{(j)}d$, $d_b^{(j)} = (1 - \Gamma^{(j)})d$, and $0 \leq \Gamma^{(j)} \leq 1$. In the direction \hat{y} the wires are limited by the sample size (which we assume to be infinite). Two layer types can occur in the MLG. Layers where $\chi_a^{(j)} \neq \chi_b^{(j)}$ will be called *structured layers* (e.g., the etched layers where the material b is vacuum), and those with $\chi_a^{(j)} = \chi_b^{(j)}$ *homogeneous layers* (e.g., the substrate).

The characteristic (common) property of all layers is the lateral periodicity d along the direction \hat{x} . Thus the susceptibility $\chi(\mathbf{r})$ can be developed into a Fourier series

$$\chi(x, z) = \sum_h \chi_h(z) e^{ihx}, \quad (1)$$

$$\chi_h(z) = \frac{1}{d} \int_{-d/2}^{d/2} dx \chi(x, z) e^{-ihx}, \quad (2)$$

with the reciprocal grating vectors $h = (2\pi/d)m$ of the grating order m (integer). The reciprocal lattice of a grating is a

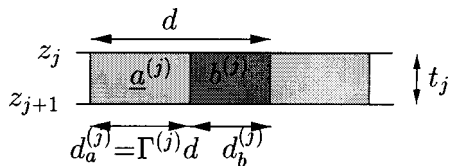


FIG. 2. Drawing of a structured layer j consisting of two wires a and b .

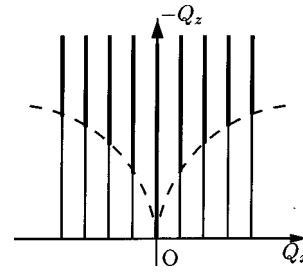


FIG. 3. Reciprocal spaces of a MLG are grating truncation rods distributed equidistantly at positions $h = (2\pi/d)m$. Only the part above the limiting Ewald spheres (represented by a thicker line) is accessible in a coplanar scattering experiment.

periodic arrangement of grating truncation rods (GTR's); see Fig. 3. They are perpendicular to the averaged surface normal. Their intersection with the Q_x axis is defined by h . In all homogeneous layers the Fourier components of $h \neq 0$ (non-zero GTR's) vanish.

III. KINEMATICAL THEORY

In this section we formulate the kinematical theory of reflection by multilayer gratings.

A. Reflection from perfect multilayer gratings

The propagation of the wave field in a grating is described by the Maxwell equations. They reduce to the scalar wave equation for x-ray reflection under grazing incidence,

$$(\Delta + K^2)E(\mathbf{r}) = V(\mathbf{r})E(\mathbf{r}). \quad (3)$$

This can be solved by use of Green's functions.^{10,15} This leads to an integral equation for the amplitudes of the scattered waves. Restricting ourselves to the first iterative solution, we obtain the first Born approximation with the kinematical scattering integral

$$E_s(\mathbf{r}) = \int d\mathbf{r}' \left(\frac{K^2}{4\pi} \right) \chi(\mathbf{r}') \frac{e^{i|\mathbf{r}-\mathbf{r}'|K}}{|\mathbf{r}-\mathbf{r}'|} E_0 e^{i\mathbf{K}\mathbf{r}'}. \quad (4)$$

This writes the amplitude of the scattered wave $E_s(\mathbf{r})$ as a single scattering process of the incident plane wave $E_0 e^{i\mathbf{K}\mathbf{r}'}$ by the susceptibility distribution $\chi(\mathbf{r}')$.

In the conventional kinematical theory, the Fraunhofer approximation is used.^{11,12} This is adequate in small samples, whose size is smaller than the first Fresnel zone. The approximation is inconvenient for laterally extended planar multilayers. Moreover, it prevents a direct comparison of the calculated amplitudes with the dynamical theory. Therefore, we solve the integral without these restrictions using the stationary phase method.

We replace the susceptibility in Eq. (4) by its Fourier series (1). Then the scattered wave field is expressed by the sum of particular amplitudes $E_s(\mathbf{r}, \mathbf{K}) = \sum_h E_h(\mathbf{r}, \mathbf{K})$, which are enumerated by the reciprocal grating vectors h . Since the particular amplitudes at different positions differ only by a phase term and the final goal is to find their intensities, it is sufficient to calculate them at one point $\mathbf{r} = 0$. It is

$$E_h \equiv E_h(\mathbf{r}=0, \mathbf{K}) = \frac{K^2}{4\pi} E_0 \int dz \chi_h(z) e^{iK_z z} U_h(z, \mathbf{K}), \quad (5)$$

which contains the integral

$$U_h(z, \mathbf{K}) = \int \int d\mathbf{r}_{\parallel} \frac{1}{|\mathbf{r}_{\parallel}|} e^{i(\mathbf{K}_{h\parallel} \mathbf{r}_{\parallel} + K|\mathbf{r}_{\parallel}|)}. \quad (6)$$

Here we defined the lateral wave-vector components $\mathbf{K}_{h\parallel}$ by the (two-dimensional) Bragg law for gratings (grating equation¹⁶)

$$\mathbf{K}_{h\parallel} = \mathbf{K}_{\parallel} + \mathbf{h}. \quad (7)$$

The two-dimensional stationary phase method^{17,18} is employed to evaluate the integral $U_h(z, \mathbf{K})$, which gives

$$U_h(z, \mathbf{K}) = \frac{2\pi i}{K_{hz}} e^{iK_{hz}z}, \quad (8)$$

with

$$K_{hz} = \sqrt{K^2 - |\mathbf{K}_{h\parallel}|^2}. \quad (9)$$

The reflected wave field above the sample is a fan of diffracted-reflected plane waves (Fig. 1), diffracted by the reciprocal vector \mathbf{h} and reflected back toward the vacuum with the wave vector [Eqs. (7) and (9)]

$$\mathbf{K}_h = \mathbf{K}_{h\parallel} - K_{hz} \hat{z} = (K_{hx}, K_y, -K_{hz}). \quad (10)$$

Their amplitudes on the sample surface [Eqs. (5) and (8)] are

$$E_h = E_0 \frac{iK^2}{2K_{hz}} \int dz \chi_h(z) e^{-iQ_{hz}z}, \quad (11)$$

where the vacuum wave-vector transfer is

$$\mathbf{Q}_h = \mathbf{K}_h - \mathbf{K}. \quad (12)$$

Following the condition $K^2 - |\mathbf{K}_{h\parallel}|^2 > 0$ the kinematically scattered wave field consists only of waves with real K_{hz} (in contrary the dynamical theory considers also the evanescent waves, i.e., the waves with imaginary K_{hz}).

Finally, the reflection amplitude is $R_h = E_h/E_0$ and the sample reflectivity defined as a ratio of the energy fluxes is

$$\mathcal{R}_h = |R_h|^2 \frac{K_{hz}}{K_z}. \quad (13)$$

Reflection by a multilayer grating

Equation (11) allows us to calculate the XRR from any grating structure characterized by any profile of the susceptibility. Now let us consider a MLG whose Fourier coefficients of the susceptibility are constant in each layer j . Then it is

$$\chi_h(z) = \sum_{j=1}^N \chi_h^{(j)} [H(z-z_j) - H(z-z_{j+1})], \quad (14)$$

where the index j goes over all layers of the multilayer, $\chi_h^{(j)}$ is the Fourier coefficient of the susceptibility in the j th layer,

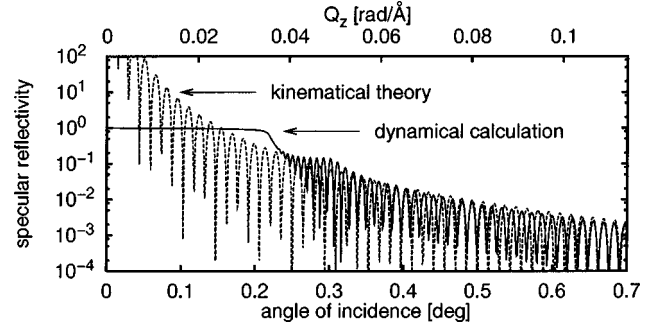


FIG. 4. Comparison of the dynamical and kinematical calculations of the specular reflectivity curves (the main truncation rod) of the discussed GaAs surface grating (period 8000 Å, wire width to grating period $\Gamma = 0.5$, thickness 3000 Å, wavelength 1.54 Å).

and $H(z)$ is the Heaviside (step) function. Integral (11) turns into the sum over the contributions of the horizontal interfaces

$$E_h = E_0 \sum_{j=1}^N \tau_{h,j}^{\text{kin}} e^{-iQ_{hz}z_j}. \quad (15)$$

Here we generalize the *kinematical Fresnel reflection coefficient for a periodically structured interface j* ,

$$\tau_{h,j}^{\text{kin}} \equiv \frac{K^2 (\chi_h^{(j-1)} - \chi_h^{(j)})}{-2K_{hz} Q_{hz}}. \quad (16)$$

In the case of specular reflection ($h=0$, $Q_{0z} = -2K_{0z}$) the coefficient $\tau_{0,j}^{\text{kin}}$ coincides perfectly with the *kinematical Fresnel reflection coefficient* of a planar interface between two homogeneous layers with averaged susceptibilities

$$\tau_j^{\text{kin}} = \frac{K^2}{Q_z^2} (\chi_0^{(j-1)} - \chi_0^{(j)}). \quad (17)$$

The specular curve of the grating is identical to that of an associated *laterally averaged* planar multilayer. The kinematical theory neglects refraction as well as total external reflection and any case of extinction. As a consequence the calculated reflectivity (Fig. 4) diverges toward small incident angles, and does not reproduce the refraction shift observed in the experiments.

The generalized Fresnel coefficients of the nonspecular (higher-order) GTR's $h \neq 0$ are proportional to the contrast between the Fourier coefficients of the susceptibilities of the two subsequent layers ($\chi_h^{(j-1)} - \chi_h^{(j)}$).

For GTR's with $\chi_h^{(j)} = 0$, the kinematical theory predicts zero intensity; these GTR's are kinematically forbidden. Otherwise, $\tau_{h,j}^{\text{kin}}$ is inversely proportional to the vertical components of the scattering vector Q_{hz} and of the diffracted wave vector K_{hz} . Figures 5 and 6 show the calculated intensity profiles.

B. Kinematical reflection from rough multilayer gratings

In a multilayer grating we find the phenomena of interface roughness between different layers similar to planar multilayers. Moreover, there occur defects of the grating shape created during the etching process (Fig. 7).

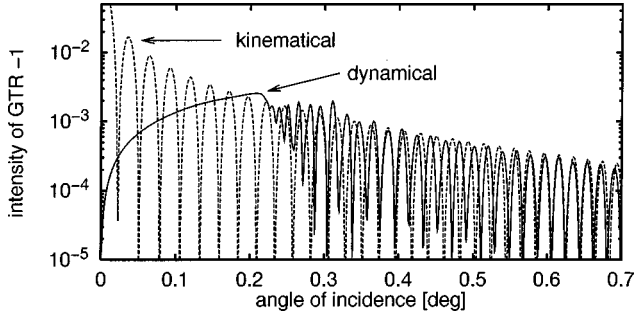


FIG. 5. Comparison of the kinematical and dynamical calculations of the grating truncation rod -1 for the surface grating described in Fig. 4.

The defects on the top of the grating and in the grooves can be interpreted as horizontal surface roughness, which will be described together with the interface roughness. The sidewall roughness will be considered independently. Here we restrict ourselves on the discussion of the influences on the coherent intensity.

1. Rough sidewalls

Let us suppose that the sidewalls, i.e., the walls separating the materials $a^{(j)}$ and $b^{(j)}$ in each layer, are rough. The lateral positions of the side walls of the n th wire in the j th layer are $nd \pm d_a^{(j)}/2 + v^{(j,n)}(\mathbf{r})$, where the displacement $v^{(j,n)}$ is a

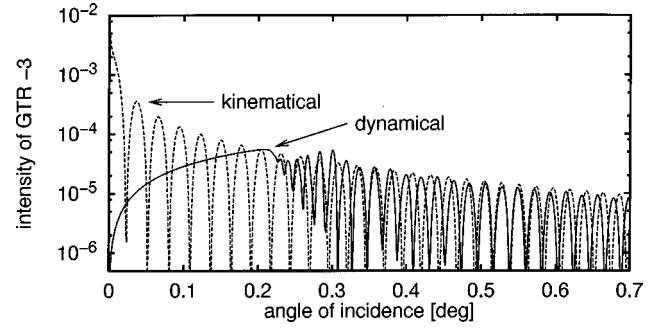


FIG. 6. Comparison of the kinematical and dynamical calculations of the GTR -3 .

random quantity. This modifies the lateral Fourier coefficients of the susceptibilities changing the reflection amplitudes (15) and Fresnel coefficients (16). Assuming no correlation among the sidewall fluctuations of different wires, we apply the coherent approach calculating the reflection amplitudes for a scattering potential laterally averaged over the statistical ensemble of the sidewall positions.

The rough side walls do not influence the kinematical intensity of the specular truncation rod. The corresponding Fresnel coefficient is proportional to the zeroth Fourier component of the susceptibility, which is already the laterally averaged susceptibility in the layer. Consequently we can concentrate on GTR's with $h \neq 0$. Averaging the Fourier component $\chi_h^{(j)}$ gives

$$\langle \chi_h^{(j)} \rangle_v = (\chi_a^{(j)} - \chi_b^{(j)}) \left\langle \frac{1}{d} \int_{-d_a/2+v^{(j)}}^{d_a/2+v'^{(j)}} dx e^{-ihx} \right\rangle_v = (\chi_a^{(j)} - \chi_b^{(j)}) \langle e^{-ihv} \rangle_v. \quad (18)$$

We assume a Gaussian distribution function of the side wall roughness characterized by the root mean square roughness $\sigma_v^{(j)}$. Then the coefficients are diminished by Debye-Waller-like factors

$$\langle \chi_h^{(j)} \rangle_v = \chi_h^{(j)} \cdot e^{-h^2(\sigma_v^{(j)})^2/2}, \quad (19)$$

$$\langle \mathbf{r}_{h,j}^{\text{kin}} \rangle_v = \frac{K^2}{-2K_{hz}Q_{hz}} (\langle \chi_h^{(j-1)} \rangle_v - \langle \chi_h^{(j)} \rangle_v). \quad (20)$$

Depending directly on h , the Debye-Waller factor $e^{-h^2\sigma_v^2/2}$ progressively damps the higher-order truncation rods. In order to decrease the GTR's noticeably near to the specular rod, the factor $h\sigma_v$ should be at about unity, and therefore $\sigma_v \gtrsim d/4$. For a grating periodicity of $1 \mu\text{m}$ the intensity of the first GTR changes essentially for a roughness of several hundreds \AA . Its reflectivity is not sensitive to the small roughness of several \AA .

2. Rough horizontal interfaces

The position $z_j(\mathbf{r})$ of a rough interface j is random, $z_j(\mathbf{r}) = z_j + u_j(\mathbf{r})$; see Fig. 7. Also, here we apply the coherent approach, where the reflection amplitudes are averaged over the statistical ensemble of random interface positions. Therefore, Eq. (15) has to be averaged:

$$\langle E_h(\mathbf{r}) \rangle = \left\langle E_0 \sum_{j=1}^N \mathbf{r}_{h,j}^{\text{kin}} e^{-iQ_{hz}z_j(\mathbf{r})} \right\rangle = E_0 \sum_{j=1}^N \langle \mathbf{r}_{h,j}^{\text{kin}}(\mathbf{r}) \rangle e^{-iQ_{hz}z_j}. \quad (21)$$

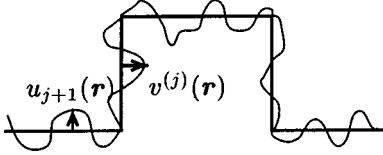


FIG. 7. Drawing of a layer in a rough MLG with random fluctuations of the horizontal interfaces $u_{j+1}(\mathbf{r})$ and the sidewalls $v^{(j)}(\mathbf{r})$.

Making use of the Gaussian probability distribution function with a rms roughness σ_j , we obtain the effective kinematical Fresnel coefficients for rough horizontal interface j

$$\langle \tau_{h,j}^{\text{kin}}(\mathbf{r}) \rangle = \tau_{h,j}^{\text{kin}}(\mathbf{r}) \cdot \langle e^{-iQ_{hz}u_j(\mathbf{r})} \rangle = \tau_{h,j}^{\text{kin}} \cdot e^{-Q_{hz}^2\sigma_j^2/2}. \quad (22)$$

Similarly to the specular reflectivity from rough planar multilayers,¹³ we obtain the kinematical damping factor depending on the \hat{z} component of the vacuum scattering vector (the Debye-Waller form of the diminution).

IV. DYNAMICAL THEORY

First we solve the wave equation within one structured layer. Then we couple the wave fields in all layers by applying the boundary conditions providing the reflection amplitude for the whole MLG. Finally, we treat the reflection from rough gratings.

A. Reflectivity from perfect multilayer gratings

1. Wave field in a structured layer

Since the susceptibility $\chi(\mathbf{r})$ is periodic in the direction \hat{x} , its Fourier transform (1) is discrete and we can substitute it into the wave equation (3). Similarly to the dynamical theory of x-ray diffraction¹⁹ we assume the solution in the form of a one-dimensional Bloch (Ewald) wave

$$E(\mathbf{r}) = \sum_h e^{ik_{h\parallel}r} E_h(z), \quad (23)$$

$$\mathbf{k}_{h\parallel} = \mathbf{K}_{\parallel} + \mathbf{h}. \quad (24)$$

We introduce the corresponding wave-vector components according to the spherical dispersion relation

$$\kappa_{hz} = \sqrt{K^2 \chi_0 - \mathbf{k}_{h\parallel}^2}, \quad (25)$$

inside the layers with laterally averaged susceptibility. Then the wave equation decomposes into a set of differential equations¹⁴ for each Fourier component h ,

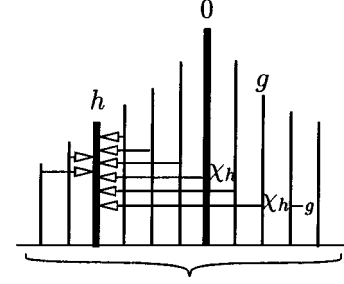


FIG. 8. Schematic drawing of the dynamical scattering processes. In the fully dynamical theory, the wave field of a truncation rod h is excited by multiple scattering from all the other truncation rods, as given by Eq. (28).

$$\kappa_{hz}^2 E_h(z) + \frac{d^2 E_h(z)}{dz^2} + K^2 \sum_{g, g \neq h} E_g(z) \chi_{h-g} = 0. \quad (26)$$

We search for the solution in the plane-wave representation with the particular solutions $E_{h,n}(z) = e^{ik_{zn}z} E_{h,n}$. The differential equation (26) is invariant with respect to the sign of k_{zn} . The total wave field in a layer j is the linear combination of the particular solutions, written in the form⁷

$$E_h^{(j)}(z) = \sum_n [e^{ik_{zn}^{(j)}(z-z_{j+1})} T_n^{(j)} + e^{-ik_{zn}^{(j)}(z-z_{j+1})} R_n^{(j)}] E_{h,n}^{(j)}, \quad (27)$$

where n goes over all the particular solutions of the differential equation (26), and the coefficients have the physical meaning of amplitudes of transmitted (T_n) and reflected (R_n) waves related to the particular solutions n . Amplitude phases are set with respect to the lower layer interface z_{j+1} .

The wave equation turns into

$$E_{h,n} = \frac{K^2}{k_{zn}^2 - \kappa_{hz}^2} \sum_{g, g \neq h} E_{g,n} \chi_{h-g}. \quad (28)$$

The amplitude $E_{h,n}$ of a particular solution n associated to a truncation rod h is proportional to the resonance factor $K^2/(k_{zn}^2 - \kappa_{hz}^2)$. The z components k_{zn} lie on a dispersion surface, which is different from the spherical one [Eq. (25)].^{8,9} This makes the resonance factors as well as the amplitudes $E_{h,n}$ in Eq. (28) finite. Further, $E_{h,n}$ depends on the dynamical contribution of all other GTR's (the so-called *intertruncation rod scattering*), as schematically represented in Fig. 8.

The summation equation (28) for the wave fields can be conveniently rewritten using the matrix formalism into an eigenvalue problem⁹

$$[\hat{A} - k_{zn}^2 \hat{I}] \vec{E}_n = \vec{0}, \quad (29)$$

$$\hat{A} = \begin{pmatrix} \ddots & & & & \\ & \kappa_{-h,z}^2 & K^2 \chi_{-h} & K^2 \chi_{-2h} & \\ & K^2 \chi_h & \kappa_{0z}^2 & K^2 \chi_{-h} & \\ & K^2 \chi_{2h} & K^2 \chi_h & \kappa_{hz}^2 & \\ & & & & \ddots \end{pmatrix}, \quad \vec{E}_n = \begin{pmatrix} \vdots \\ E_{-h,n} \\ E_{0,n} \\ E_{h,n} \\ \vdots \end{pmatrix}, \quad (30)$$

where \hat{I} is the unity matrix, and $\vec{0}$ is column vector of zeros.

The solution of Eq. (29) gives the wave-vector components k_{zn} which form the column vector \vec{k}_z . The associated column eigenvectors \vec{E}_n form the matrix \hat{E} . The vectors \vec{E}_n are unique except of a multiplicative constant [see Eq. (29)], allowing us to choose $E_{n,n}=1$ for each n . The number of solutions, i.e., the dimension of the vectors and matrices, is infinite. Many of the wave fields, mainly those of distant truncation rods, are weak. That allows us to limit the number \mathcal{D} of the GTR's involved in the numerical procedure (*multiple-beam approximation* of the dynamical theory). The dimension \mathcal{D} is chosen depending on the numerical precision.

In the following section we define for each layer j the column vectors $\vec{T}^{(j)}$, $\vec{R}^{(j)}$, and $\vec{k}_z^{(j)}$ containing T_n , R_n , and k_{zn} , respectively. The diagonal matrix of the eigenvalues $k_{z,n}$ is $\hat{k}_z^{(j)}$, and the corresponding eigenvector matrix is $\hat{E}^{(j)}$. The dimension of these vectors and matrices is \mathcal{D} .

2. Boundary conditions

In Sec. IV A 1 we expressed the wave field in a structured layer as a series of plane waves [Eqs. (23) and (27)]. In order to find the coefficients $T_n^{(j)}$ and $R_n^{(j)}$, which determine the value of the excitation of the particular solutions, we connect the wave fields in the inner layers with the wave fields in the vacuum and in the substrate. We apply the convenient matrix formalism similar to the Abèles method²⁰ for planar multilayers. Various authors use different matrix sequences to couple all inner wave fields in order to obtain the reflection amplitudes above the sample surface.^{5,7} In this paper, we present an ‘‘interface approach’’ which enables us to generalize the conventional Fresnel coefficients for the case of MLG's. Moreover, this interfacelike representation will allow us to describe the scattering from gratings with rough interfaces.

The boundary conditions couple the wave fields and their derivatives at the interfaces. Let us connect the wave fields of two neighboring layers $j-1$ and j at their common interface j at $z=z_j$ (Fig. 2).

Since the boundary conditions for the wave amplitudes and their normal derivatives hold at each point (x,y,z_j) of each interface j , the conditions for the undetermined coefficients $T_n^{(j)}$ and $R_n^{(j)}$ can be expressed by the matrix relation

$$\mathcal{P}^{(j-1)} \cdot \begin{pmatrix} \vec{T}^{(j-1)} \\ \vec{R}^{(j-1)} \end{pmatrix} = \mathcal{P}^{(j)} \mathcal{Q}^{(j)} \cdot \begin{pmatrix} \vec{T}^{(j)} \\ \vec{R}^{(j)} \end{pmatrix}, \quad (31)$$

introducing the *boundary matrices* $\mathcal{P}^{(j)}$ and the *propagation matrices* $\mathcal{Q}^{(j)}$. The boundary matrices $\mathcal{P}^{(j)}$ are

$$\mathcal{P}^{(j)} = \begin{pmatrix} \hat{E}^{(j)} & \hat{E}^{(j)} \\ \hat{E}^{(j)} \hat{k}_z^{(j)} & -\hat{E}^{(j)} \hat{k}_z^{(j)} \end{pmatrix} = \begin{pmatrix} \hat{E}^{(j)} & 0 \\ 0 & \hat{E}^{(j)} \end{pmatrix} \begin{pmatrix} \hat{I} & \hat{I} \\ \hat{k}_z^{(j)} & -\hat{k}_z^{(j)} \end{pmatrix} \quad (32)$$

for structured layers, and

$$\mathcal{P}^{(j)} = \begin{pmatrix} \hat{I} & \hat{I} \\ \hat{K}_z^{(j)} & -\hat{K}_z^{(j)} \end{pmatrix} \quad (33)$$

for homogeneous layers (including the vacuum and substrate).

The *propagation matrices* $\mathcal{Q}^{(j)}$ connect the amplitudes of the waves between the bottom and top interfaces of a layer

$$\mathcal{Q}^{(j)} = \begin{pmatrix} \mathcal{Q}^{(j)+} & \hat{0} \\ \hat{0} & \mathcal{Q}^{(j)-} \end{pmatrix}. \quad (34)$$

Here $\mathcal{Q}^{(j)\pm}$ are diagonal matrices with the diagonal vector

$$(e^{\mp i k_{1,z}^{(j)} t_j}, e^{\mp i k_{2,z}^{(j)} t_j}, \dots, e^{\mp i k_{\mathcal{D},z}^{(j)} t_j}) \quad (35)$$

for structured layers, and

$$(\dots, e^{\mp i \kappa_{-1,z}^{(j)} t_j}, e^{\mp i \kappa_{0,z}^{(j)} t_j}, e^{\mp i \kappa_{1,z}^{(j)} t_j}, \dots) \quad (36)$$

for homogeneous layers, respectively. Notice the different wave vectors in the phases: in Eq. (35) there occur the wave vectors of the particular solutions of the dynamical wave field [Eq. (28)], and in Eq. (36) occur the conventional wave vectors of homogeneous layers [Eq. (25)]. The dimension of matrices \mathcal{P} and \mathcal{Q} is $2\mathcal{D}$.

3. Generalization of the Fresnel coefficients for structured interfaces

Equation (31) can be rewritten by coupling the amplitudes at the bottom interfaces of two neighboring layers $j-1$ and j :

$$\begin{pmatrix} \vec{T}^{(j-1)} \\ \vec{R}^{(j-1)} \end{pmatrix} = \mathcal{N}_j \begin{pmatrix} \vec{T}^{(j)} \\ \vec{R}^{(j)} \end{pmatrix}, \quad (37)$$

$$\mathcal{N}_j \equiv \mathcal{P}_{j-1,j} \cdot \mathcal{Q}^{(j)}. \quad (38)$$

We introduced the ‘‘interface matrix’’

$$\mathcal{P}_{j-1,j} \equiv (\mathcal{P}^{(j-1)})^{-1} \mathcal{P}^{(j)} \equiv \begin{pmatrix} \hat{\tau}_j & \hat{\rho}_j \\ \hat{\rho}_j & \hat{\tau}_j \end{pmatrix}, \quad (39)$$

which corresponds formally to the ‘‘interface matrix’’ of the Fresnel coefficients for an interface of a planar multilayer. Notice that the boundary matrix (32) can be easily inverted:

$$(\mathcal{P}^{(j)})^{-1} = \frac{1}{2} \begin{pmatrix} \hat{I} & (\hat{k}_z^{(j)})^{-1} \\ \hat{I} & -(\hat{k}_z^{(j)})^{-1} \end{pmatrix} \begin{pmatrix} (\hat{E}^{(j)})^{-1} & 0 \\ 0 & (\hat{E}^{(j)})^{-1} \end{pmatrix}. \quad (40)$$

The matrices of dimension \mathcal{D} introduced in Eq. (39) are

$$\hat{\tau}_j = \frac{1}{2} [\hat{E}_{j-1,j} + (\hat{k}_z^{(j-1)})^{-1} \hat{E}_{j-1,j} \hat{k}_z^{(j)}],$$

$$\hat{\rho}_j = \frac{1}{2} [\hat{E}_{j-1,j} - (\hat{k}_z^{(j-1)})^{-1} \hat{E}_{j-1,j} \hat{k}_z^{(j)}], \quad (41)$$

with $\hat{E}_{j-1,j} = (\hat{E}^{(j-1)})^{-1} \hat{E}^{(j)}$. Since the wave-vector matrices \hat{k}_z are diagonal, the matrix elements are explicitly

$$\tau_{j,mn} = (E_{j-1,j})_{mn} / t_{j,mn}, \quad \rho_{j,mn} = (E_{j-1,j})_{mn} \cdot \tau_{j,mn} / t_{j,mn}, \quad (42)$$

where

$$\tau_{j,mn} = \frac{2k_{z,m}^{(j-1)}}{k_{z,m}^{(j-1)} + k_{z,n}^{(j)}}, \quad \tau_{j,mn} = \frac{k_{z,m}^{(j-1)} - k_{z,n}^{(j)}}{k_{z,m}^{(j-1)} + k_{z,n}^{(j)}} \quad (43)$$

are the *generalized Fresnel transmission and reflection coefficients for grating diffraction*. They all form the *generalized Fresnel matrices* $\hat{\tau}_j$ and $\hat{\tau}_j$. The transmission coefficients $\tau_{j,mn}$ correspond to the transmission and diffraction of the wave $k_{z,m}^{(j-1)}$ (in layer $j-1$) through the interface j into the wave $k_{z,n}^{(j)}$ in layer j .

Finally, we can write the transfer matrix in a transparent form

$$\hat{\tau}_j = \frac{\hat{k}_z^{(j-1)} - \hat{k}_z^{(j)}}{\hat{k}_z^{(j-1)} + \hat{k}_z^{(j)}} = \begin{pmatrix} \frac{k_{z,1}^{(j-1)} - k_{z,1}^{(j)}}{k_{z,1}^{(j-1)} + k_{z,1}^{(j)}} & 0 & 0 & \dots \\ 0 & \frac{k_{z,2}^{(j-1)} - k_{z,2}^{(j)}}{k_{z,2}^{(j-1)} + k_{z,2}^{(j)}} & 0 & \dots \\ 0 & 0 & \dots & \dots \end{pmatrix}. \quad (45)$$

The interface matrix reduces to the known form of a planar multilayer

$$\mathcal{P}_{j-1,j} = \frac{\hat{I}}{\hat{\tau}_j} \begin{pmatrix} \hat{I} & \hat{\tau}_j \\ \hat{\tau}_j & \hat{I} \end{pmatrix}. \quad (46)$$

4. Reflection from a multilayer grating

Above, we have coupled the wave fields at the bottom interfaces of two subsequent layers by the transfer matrices \mathcal{N}_j [Eq. (37)]. Finally we couple the wave fields in the vacuum (index $v=0$) and in the substrate (index $s=N$) by the transfer matrix of the whole multilayer \hat{M} :

$$\begin{pmatrix} \vec{T}^v \\ \vec{R}^v \end{pmatrix} = \hat{M} \cdot \begin{pmatrix} \vec{T}^s \\ \vec{R}^s \end{pmatrix}, \quad (47)$$

$$\hat{M} = \prod_{j=1}^N \mathcal{N}_j \equiv \begin{pmatrix} \hat{M}_{11} & \hat{M}_{12} \\ \hat{M}_{21} & \hat{M}_{22} \end{pmatrix}.$$

We employ two additional conditions:

(1) Since the incident wave is planar, all elements \vec{T}^v are zero except that corresponding to the incident beam $h=0$, which is unity; $\vec{T}^v = (0, \dots, 0, 1, 0, \dots, 0)$.

(2) The substrate is semi-infinite, and no reflected waves are excited ($\vec{R}^s = \vec{0}$).

Then the amplitudes of the reflected waves above the sample surface are

$$\vec{R}^v = \hat{M}_{21} \cdot \hat{M}_{11}^{-1} \cdot \vec{T}^v, \quad (48)$$

$$\mathcal{P}_{j-1,j} = \frac{\hat{E}_{j-1,j}}{\hat{\tau}_j} \otimes \begin{pmatrix} \hat{I} & \hat{\tau}_j \\ \hat{\tau}_j & \hat{I} \end{pmatrix}. \quad (44)$$

The matrix operations $\hat{a} \otimes \hat{b}$ and \hat{a}/\hat{b} used here are the element-by-element multiplication and division operators, respectively [i.e., $(\hat{a} \otimes \hat{b})_{ij} \equiv a_{ij} b_{ij}$ and $(\hat{a}/\hat{b})_{ij} \equiv a_{ij}/b_{ij}$].

Let us consider the special case of an interface separating two homogeneous layers. There is no lateral diffraction in these layers; therefore, $\hat{E}^{(j-1)}$, $\hat{E}^{(j)}$ and $\hat{E}_{j-1,j}$ are unity matrices. The matrices $\hat{\tau}_j = \hat{\tau}_j$ and $\hat{\rho}_j = \hat{\tau}_j$ are diagonal and their elements correspond to the classical Fresnel coefficients²¹

where the vector \vec{R}^v is the column vector of the matrix $(\hat{M}_{21} \cdot \hat{M}_{11}^{-1})$ corresponding to the column of $h=0$. The reflected intensity of the wave h is $|R_h^v|^2$ and the grating reflectivity is

$$\mathcal{R}_h = |R_h^v|^2 \frac{K_{hz}}{K_z}. \quad (49)$$

In summary, we expressed the problem of the scattering from a MLG by a matrix formalism similar to the matrix formalism of reflection from planar multilayers by generalizing the Fresnel reflection and transmission coefficients. However, the matrices employed here are of higher order. Figures 5 and 6 show the intensity profiles for some odd-order GTR's, and Fig. 9 those for even-order GTR's.

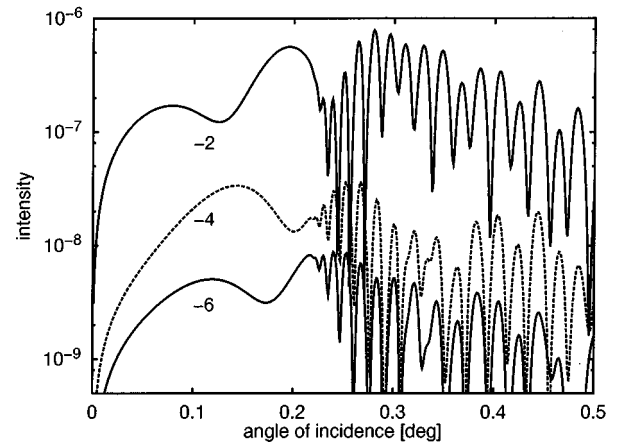


FIG. 9. The kinematically forbidden even-order truncation rods -2 , -4 , and -6 , calculated by the dynamical theory. The kinematical theory gives zero reflectivity of even-order GTR's for a grating with the ratio $\Gamma=0.5$.

B. Reflection from rough multilayer gratings

In this section we treat the influence of the roughness on the intensity profile of the truncation rods.

1. Rough sidewalls

In the kinematical theory the amplitudes of the scattered waves were found to be proportional to the Fourier transformation of the susceptibility (17). The roughness of the sidewalls has been taken into account by laterally averaging the Fourier coefficients.

We can include averaged Fourier coefficients in the dynamical procedure that modifies the dispersion relation (28) and also influences the resonance factor. The interaction among distant GTR's will be exponentially reduced, and thus the dynamical effects will be diminished.

As in the kinematical theory we find that the intensity of the low-order GTR's is not affected essentially by the roughness of the grating sidewalls below several hundred Å. In order to be sensitive to this roughness, we would have to measure the scattered intensity in a geometry where the incident beam is nearly parallel to the wires. Such a noncoplanar scattering geometry requires another experimental arrangement. This case is promising and it will be studied in the future.

2. Rough horizontal interfaces

The rough interfaces cause layer thickness fluctuations which influence randomly the phase terms [Eq. (35)] of the propagation matrices $Q^{(j)}$ [Eq. (34)] by the factor $\Phi_j(r_{\parallel}) = e^{ik_z^{(j)}t_j(r_{\parallel})} = \Phi_j e^{ik_z^{(j)}(u_{j+1}(r_{\parallel}) - u_j(r_{\parallel}))}$. Therefore the propagation matrix also becomes random

$$Q^{(j)}(r_{\parallel}) = \mathcal{U}_j(-k_z^{(j)}, r_{\parallel}) Q^{(j)}(k_z^{(j)}) \mathcal{U}_{j+1}(k_z^{(j)}, r_{\parallel}), \quad (50)$$

with

$$\mathcal{U}_j(k_z, r_{\parallel}) \equiv \begin{pmatrix} \mathcal{U}^{(j)+}(k_z, r_{\parallel}) & 0 \\ 0 & \mathcal{U}^{(j)-}(k_z, r_{\parallel}) \end{pmatrix}. \quad (51)$$

$\mathcal{U}^{(j)\pm}(k_z, r_{\parallel})$ are the diagonal matrices, with the diagonal vector

$$(e^{\mp ik_{1,z}u_j(r_{\parallel})}, e^{\mp ik_{2,z}u_j(r_{\parallel})}, \dots, e^{\mp ik_{D,z}u_j(r_{\parallel})}) \quad (52)$$

for structured layers.

The amplitudes of the reflected waves given by Eq. (48) have to be averaged over the random interface displacements. We employ the approximation

$$\langle \vec{R}^v \rangle = \langle \hat{M}_{21} \cdot \hat{M}_{11}^{-1} \cdot \vec{T}^v \rangle \approx \langle \hat{M}_{21} \rangle \cdot (\langle \hat{M}_{11} \rangle)^{-1} \cdot \vec{T}^v. \quad (53)$$

The averaged transfer matrix of the whole multilayer reads [cf. Eq. (47)]

$$\langle \mathcal{M}(r_{\parallel}) \rangle = \prod_{j=1}^N \langle \mathcal{N}_j(r_{\parallel}) \rangle = \prod_{j=1}^N \langle \mathcal{P}_{j-1,j}(r_{\parallel}) \rangle Q^{(j)}, \quad (54)$$

where we renamed the ideal matrices $\mathcal{P}_{j-1,j}$ in Eq. (39) as $\mathcal{P}_{j-1,j}^{\text{id}}$ and put

$$\mathcal{P}_{j-1,j}(r_{\parallel}) \equiv \mathcal{U}_j(k_z^{(j-1)}, r_{\parallel}) \mathcal{P}_{j-1,j}^{\text{id}} \mathcal{U}_j(-k_z^{(j)}, r_{\parallel}). \quad (55)$$

Averaging the boundary matrix is straightforward. It leads to the form where the elements of the ideal matrix are multiplied by the characteristic function χ_{u_j} of the probability distribution of interface displacements [as usual, we can use the Gaussian distribution function $\chi_{u_j}(Q) = e^{-Q^2\sigma_j^2/2}$]

$$\langle \mathcal{P}_{j-1,j}(r_{\parallel}) \rangle = \begin{pmatrix} [\tau_{j,mn} \chi_{u_j}(k_{z,m}^{(j-1)} - k_{z,n}^{(j)})] & [\rho_{j,mn} \chi_{u_j}(k_{z,m}^{(j-1)} + k_{z,n}^{(j)})] \\ [\rho_{j,mn} \chi_{u_j}(-k_{z,m}^{(j-1)} - k_{z,n}^{(j)})] & [\tau_{j,mn} \chi_{u_j}(k_{z,m}^{(j)} - k_{z,n}^{(j-1)})] \end{pmatrix}. \quad (56)$$

This relation is a generalization of the averaged boundary matrix for XRR by a rough planar interface

$$\langle \mathcal{P}_{j-1,j}(r_{\parallel}) \rangle = \frac{1}{t_j} \begin{pmatrix} \chi_{u_j}(k_z^{(j-1)} - k_z^{(j)}) & \tau_j \chi_{u_j}(k_z^{(j-1)} + k_z^{(j)}) \\ \tau_j \chi_{u_j}(-k_z^{(j-1)} - k_z^{(j)}) & \chi_{u_j}(k_z^{(j)} - k_z^{(j-1)}) \end{pmatrix}, \quad (57)$$

where the Fresnel coefficients τ_j and t_j have now their ‘‘classical’’ meaning.

Comparing the matrix elements (56) to the definition (42) we find the generalized Fresnel coefficients for rough interfaces in gratings

$$\begin{aligned} \langle \tau_{j,mn}(r_{\parallel}) \rangle &= \tau_{j,mn} e^{-2k_{z,m}^{(j)} k_{z,n}^{(j-1)} \sigma_j^2}, \\ \langle t_{j,mn}(r_{\parallel}) \rangle &= t_{j,mn} e^{(k_{z,m}^{(j)} - k_{z,n}^{(j-1)})^2 \sigma_j^2/2}. \end{aligned} \quad (58)$$

Notice the different meaning of the generalized Fresnel coefficients τ and t [determined by Eq. (43)] and of the coefficients τ and ρ [determined by Eqs. (39) and (42)]. The Fresnel coefficients τ_j and t_j of one interface j can be interpreted as the structure factor for the scattering from one dif-

fraction order m to another order n at that interface. The coefficients τ and ρ describe the transfer of the waves from one grating diffraction order to the other, which also considers the influence of all the other scattering processes at this interface. Figure 10 shows the calculated GTR profiles for MLG's with different interface roughnesses.

C. Numerical implementation

Up to now we have provided a theoretical description of the dynamical theory for rough gratings. Before discussing numerical results, also in comparison with the kinematical theory, we briefly summarize the procedure and formulas, which are suitable for the numerical implementation of the dynamical theory.

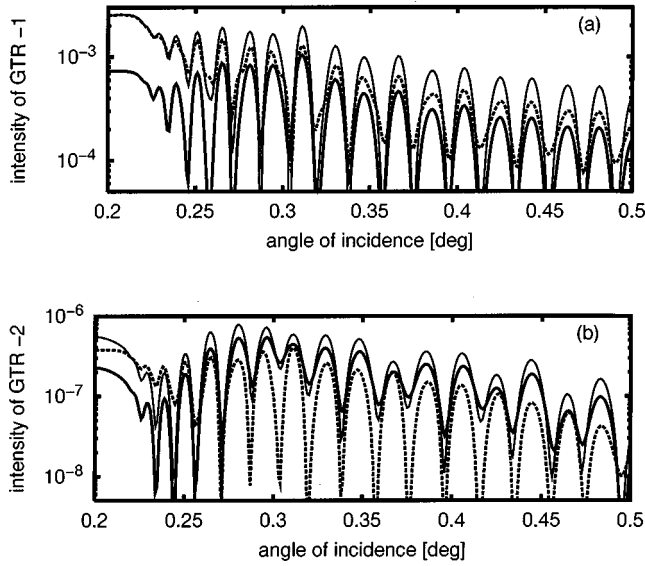


FIG. 10. Intensity of (a) the odd-order truncation rod -1 , and (b) the even-order truncation rod -2 of the surface grating described in Fig. 4 with rough interfaces. Thin full curve: no roughness. Dashed curve: no surface roughness, interface roughness 12 \AA . Thick full curve: surface roughness 12 \AA , no interface roughness. Notice that the reflectivity curve from the perfect MLG is not damped, while the other two curves have the same order below the critical angle, and opposite order above it. The explanation of this phenomena is given in the discussion.

First of all, the z components of the wave vectors of the diffracted waves are calculated. For homogeneous layers (including vacuum and substrate) they are simply given by the spherical dispersion relation (25). For structured layers, that requires solving the eigenvalue problem (29) with the Fourier coefficients of susceptibility (2). The eigenvectors form the matrices $\hat{E}^{(j)}$, which are unity matrices for homogeneous layers.

The interface matrices of all interfaces (39) are formed by the elements (42), which are corrected, in case of roughness, according to Eq. (56). Then the transfer matrix of the whole multilayer is determined by multiplying successively the propagation matrices of the interfaces and layers using Eqs. (38) and (47). Finally, the grating reflectivity (49) is obtained independently for each grating truncation rod. The number of dynamically interacting GTR's is chosen in the way to achieve good numerical convergence for all GTR regions of interest. Please notice that the susceptibility, the z components of the wave vectors and the amplitudes of the wave field are within the grating complex numbers; therefore all matrices are complex too.

V. DISCUSSION

A. Diffraction by ideal gratings

In the following we want to discuss the results of both theories. The dynamical theory as well as the kinematical theory reproduce a coherent grating diffraction pattern consisting of a specular rod and grating truncation rods (Fig. 3), determined by the lateral Bragg law [Eq. (7)]. The GTR's are arranged equidistantly in reciprocal space around the specular rod in a plane defined by the surface normal and the wire

normal. We remind the reader that in coplanar reflection geometry the grating period d , the wavelength used, and the horizon of the sample determine the smallest accessible Q_z value of a given GTR (above the limiting Ewald spheres in Fig. 3).

In both theories we generalize the Fresnel coefficients for the case of diffraction by structured interfaces. In the limit of a nonstructured interface between two homogeneous layers these reduce to the classical Fresnel coefficients. The *kinematical contribution* of one structured interface to the diffracted amplitude of one GTR is *directly* proportional to the corresponding generalized kinematical Fresnel coefficient (15). The diffracted wave of the whole multilayer is described by the simple series of the phase corrected Fresnel diffraction coefficients of all interfaces. That means, there are (1) no interaction of different GTR's and (2) no multiple scattering between different interfaces taken into account. Only one scattering process, the *primary scattering* from the incident wave into the considered grating diffraction order, plays a role. In the simple example of a simple square-shaped surface grating (with two structured interfaces), thickness interference fringes are created along the specular scan (Fig. 4), similar to the reflection by a laterally averaged layer, and also along the higher-order GTR's (Figs. 5 and 6), similar to the diffraction by a crystalline layer. Since any extinction effect is neglected, all GTR intensities diverge, if the vertical momentum transfer Q_z goes to zero (see Fig. 4). Notice, that the reflection curves of the nonzero GTR's in Figs. 5 and 6 merely do not diverge, since there it always $Q_{hz} \gg 0$.

The *dynamical contribution* of one structured interface depends on the *whole* generalized Fresnel matrices (39), which include the Fresnel diffraction coefficients as their elements (42). The generalized Fresnel matrices include the *primary diffraction* (scattering of the directly transmitted wave into the selected diffraction order) of the j th interface by $\tau_{j,0m}$. The *intertruncation rod scattering*, i.e., the multiple scattering among the wave fields of all GTR's (see Fig. 8), has been taken into account by the Fresnel coefficients of all the other indices $n \neq 0: \tau_{j,nm}$. Each structured interface gives rise to intertruncation rod scattering. In contrast, all planar interfaces (below the grating) contribute only by Fresnel coefficients with identical indices $[\tau_{j,mm}; \text{Eq. (46)}]$. In other words, planar interfaces exclusively cause *intratruncation rod scattering*—the dynamical interaction between the transmitted and reflected waves of the wave field of a particular GTR order. In summary, the dynamical theory takes the refraction in the layers into account. It also includes all those diffraction orders with nonreal wave vectors describing their evanescent wave character (extinction). In the specular rod one observes a plateau of total external reflection similar to specular reflection by a planar multilayer (Fig. 4). The refraction and the evanescent wave behavior of the incident and the primary diffracted waves leads to the Yoneda-like wings and Bragg-like peaks in the nonzero GTR's (similar to the grazing incidence diffraction curves of crystals²² or non-specular x-ray reflection curves of rough surfaces²³). The evanescent waves of other strongly diffracting GTR's can also affect the intensity profile of near-neighboring GTR's by intertruncation rod scattering. For example one can observe the influence of intertruncation rod scattering on the

specular scan just when the incident angle excites the Yoneda-like wing of the GTR +1. Along the GTR of weak primary scattering (weak Fresnel coefficients $\tau_{j,0m}$) the dynamical intertruncation rod scattering plays an essential role. For example, for rectangularly shaped gratings with a relative wire width $\Gamma = \frac{1}{2}$ all even-order truncation rods $2m \neq 0$ are kinematically forbidden: $\tau_{j,0,2m} = 0$. Simulations by the dynamical approach give diffraction curves with nonzero intensity (Fig. 9). There the whole diffraction intensity is of *purely dynamical origin*, caused by the intertruncation rod scattering of the nonzero GTR's into the direction of a forbidden GTR.

B. Influence of interface roughness

Interface roughness diminishes all Fresnel diffraction coefficients, kinematical [Eq. (22)] as well as dynamical [Eq. (58)] ones. Let us further discuss the dynamical theory only.

The roughness damps the primary scattering as well as the inter-GTR scattering. The reflection and transmission coefficients corresponding to primary specular reflection $\tau_{j,00}$ and $t_{j,00}$ depend on horizontal roughness in the same way as the classical Fresnel reflection and transmission coefficients of planar multilayers: below the critical angle the reflection coefficients are not affected; above they decrease with increasing Q_{0z} . The behavior of the other matrix elements of intratruncation rod scattering (diagonal terms) is more subtle. From the matrix relations (57) and (58) we deduce, especially, that the transmission coefficients are not substantially influenced for large exit angles of the corresponding diffraction order, since the vertical distance $k_{z,m} - k_{z,n}$ is small. The decrease of the reflection coefficients $\tau_{j,mn}$ is given by the static Debye-Waller-like factor which depends on the wave-vector transfer $k_{z,m}^{(j)} + k_{z,n}^{(j+1)}$, which decreases progressively with increasing angles of incidence and exit.

Numerical results are shown in Fig. 10 for the strong GTR -1 and for the kinematically forbidden second-order GTR. In both cases we calculated the curves (1) for a smooth surface grating, (2) assuming a rough interface and a smooth surface, and (3) assuming a smooth interface and a rough surface. In the *specular GTR* (not shown here) the results are comparable to the well-known features of a single-layer system: above the critical angle the surface roughness decreases the whole reflected intensity, while the interface roughness damps mainly the fringe amplitudes. For the *strong GTR orders* [e.g., -1; see Fig. 10(a)] and incident angles above the critical angle, we observe a qualitatively similar behaviour. Here primary scattering (given by $\tau_{j,0m}$) dominates the other scattering processes. In contrast to the specular rod, surface roughness also decreases the GTR intensity at incident angles *below* the critical angle. At small incident angles, $k_{z,0}$ is imaginary (evanescent wave behavior); however, the wave vectors $k_{z,m}$ of all excited negative GTR orders correspond to exit angles above the critical angle. Consequently the wave-vector transfer $q_{z,m0} = k_{z,m} + k_{z,0}$ never becomes purely imaginary, and the exponential damping factor is always smaller than unity. Therefore, the reflected intensity from a MLG with a rough surface is also below the critical angle reduced [thick full curve in Fig. 10(a)]. That is different in the second case [smooth surface and rough interface;

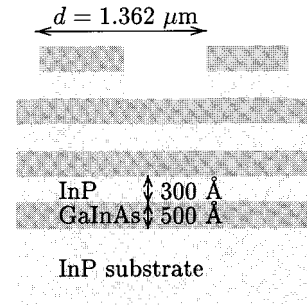


FIG. 11. Schematic drawing of the sample.

dashed curve in Fig. 10(a)]. Now the evanescent incident wave does not penetrate into the grating, and thus does not reach the second interface. Only the surface contributes to the diffraction below the critical angle.

Finally, for the *weak (kinematically forbidden) GTR orders* [e.g., GTR -2 in Fig. 10(b)] the primary scattering vanishes: $\tau_{j,0m} = 0$. The wave fields of forbidden GTR's are created by multiple scattering of the GTR's excited by the primary scattering of the incident wave. The influence of a rough surface [thick full curve in Fig. 10(b)] and a rough interface (dashed curve) is similar to that of strong GTR's for small incident angles only, and it is opposite above the critical angle.

VI. EXPERIMENT

In this section we present experimental results from a partially etched multilayer grating and its evaluation by our theoretical approach. A $\text{Ga}_{1-x}\text{In}_x\text{As}/\text{InP}$ multilayer of three and a half periods (seven layers) has been grown by chemical beam evaporation on an InP [001] substrate. The bilayer sequence consists of nominally 50-nm $\text{Ga}_{0.47}\text{In}_{0.53}\text{As}$ and 30-nm InP. A surface grating with a lateral period of 1.360 μm has been fabricated by holographic exposition of a photoresist and subsequent selective etching. The etching has been stopped at the second interface; see Fig. 11. Thus the grating depth is exactly the bilayer thickness of the uppermost multilayer period. As a result, we obtained a partially etched multilayer surface grating.

The reflectivity measurements have been performed at the Optics beamline D5 at the European Synchrotron Radiation Facility in Grenoble using the setup of the high-resolution x-ray diffractometer. A single reflection Si(111) monochromator was mounted on the first goniometer, the sample on the second one, and the Si(111) analyzer crystal on the third one. The detector unit was completed by additional slits mounted in front of the analyzer in order to limit the extension of the analyzer streak. The movements of the slit, the analyzer, and the detector, as well as the whole third goniometer, were coupled in order to detect all scattered waves under identical intrinsic geometrical conditions of the whole detector unit, keeping its resolution function constant during the relatively large angular scans. We used the wavelength $\lambda = 0.7114 \text{ \AA}$. The sample was mounted in coplanar scattering geometry with a horizontal scattering plane. Figure 12 shows an ω scan at $2\theta = 0.7^\circ$, with a central specular peak and first-order grating reflection orders. The specular peak as well as the GTR peaks are well localized with a full width at

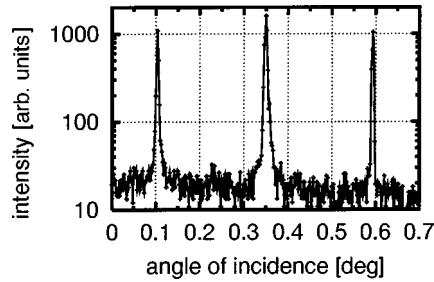


FIG. 12. Measured ω scan for $2\theta=0.7^\circ$ of the sample which cuts the truncation rods -1 , 0 , and $+1$.

half maximum of 0.005° . From their positions in reciprocal space, $Q_x^{\pm 1} = \pm(4.61 \times 10^{-4} \pm 2 \times 10^{-6} \text{ \AA}^{-1})$, we could determine very precisely the grating period of $d = 2\pi/|Q_x^{\pm 1}| = (1.362 \pm 0.005) \mu\text{m}$. In order to avoid errors caused by the quite different precision of the participating motors during a single off-specular Q_z scan, the intensity pattern along each GTR was mapped by performing off-specular Q_z/ω maps in the narrow regions around their theoretical position. The GTR pattern was deduced by following the maximum of the small ω scans. In Fig. 13, we plot the specular reflectivity and the intensity profile of the GTR -1 . The intensity pattern of the GTR $+1$ was within the measurable accuracy identical, indicating a symmetrical shape of the wires. The curves were fitted by employing the dynamical theory. Despite of dynamical intertruncation rod scattering the non-specular GTR's are only influenced by the etched part of the multilayer, and are not sensitive to the planar multilayer at the bottom of the grating. No influence of sidewall roughness could be established, since the lower GTR orders are less sensitive to sidewall roughness (see Secs. III B1 and IV B1). However, in order to obtain a good agreement between experimental and calculated curves, we had to take the interface roughness into account. We determined the layer thicknesses close to the nominal values: $t_{\text{InP}} = 29 \pm 0.8 \text{ nm}$ and $t_{\text{Ga}_{1-x}\text{In}_x\text{As}} = 50.3 \pm 0.8 \text{ nm}$, and a rms roughness of $0.5 \pm 0.3 \text{ nm}$. The ratio of the wire width and the grating period was determined to be $\Gamma = d_A/d = 0.66 \pm 0.03$.

VII. CONCLUSION

We reported x-ray reflection from multilayer gratings, described by kinematical and dynamical theories. In the dynamical theory we proceeded by the modal eigenvalue approach. The matrix sequence was organized in such a way

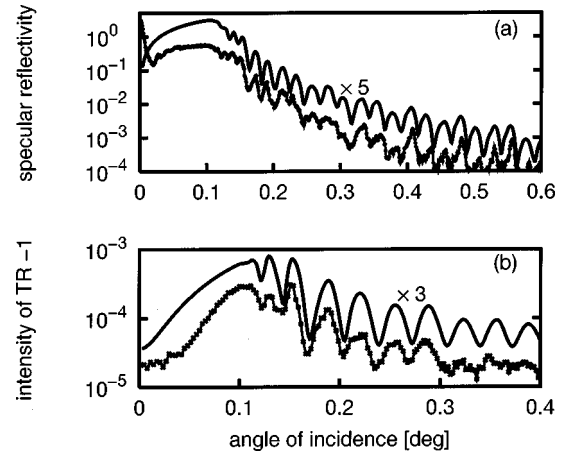


FIG. 13. Fit of the measured intensity profile of the specular (a) and -1 (b) GTR's of the sample. The simulated curves in (a) and (b) are shifted five and three times, respectively.

that the boundary matrices (describing the transition of the wave fields through the interfaces) are easily related to the introduced generalized dynamical Fresnel reflection coefficients of lateral diffraction. In the framework of the kinematical theory, we employed the stationary phase method for an evaluation of the kinematical scattering integral. We defined generalized kinematical Fresnel reflection coefficients of structured interfaces.

In both theories we considered the roughness of the horizontal planar interfaces and the vertical sidewalls. In the kinematical theory damping factors for the generalized Fresnel coefficients are obtained. In the dynamical approach the effective Fresnel diffraction coefficients of rough interfaces diminished the elements of the boundary matrices. Significantly different effects of surface roughness and interface roughness on intense GTR's and on weak (kinematically forbidden) GTR's were discussed by numerical examples. Finally, we employed the dynamical calculation for fitting the structure parameters of a partially etched GaAs/InP periodic multilayer grating.

ACKNOWLEDGMENTS

The authors would like to thank M. Gailhanou, U. Marti, and J. F. Carlin from the Ecole Polytechnique de Lausanne for the fabrication of the sample. This work was supported by Grant No. VS 96102 of the Ministry of Education of the Czech Republic and by the Deutsche Forschungsgemeinschaft (Grant No. BA1642/1-1).

¹D. Maystre, in *Progress in Optics XXI*, edited by E. Wolf (North-Holland, Amsterdam, 1984).

²M. Tolan, G. König, L. Brügemann, W. Press, F. Brinkop, and J. P. Kotthaus, *Europhys. Lett.* **20**, 223 (1992).

³M. Tolan, G. Vacca, S. K. Sinha, Z. Li, M. Rafailovich, J. Sokolov, H. Lorenz, and J. P. Kotthaus, *J. Phys. D* **28**, A231 (1995).

⁴M. Tolan, W. Press, F. Brinkop, and J. P. Kotthaus, *Phys. Rev. B* **51**, 2239 (1995).

⁵M. Nevrière, *J. Opt. Soc. Am. A* **11**, 1835 (1994).

⁶Ki-Tung Lee and T. F. George, *Phys. Rev. B* **31**, 5106 (1985).

⁷A. Sammar, J.-M. André, and B. Pardo, *Opt. Commun.* **86**, 245 (1991).

⁸V. Martynov, B. Vidal, P. Vincent, M. Brunel, D. V. Roschupkin, Yu. Agafonov, A. Erko, and A. Yuakshin, *Nucl. Instrum. Methods Phys. Res. A* **339**, 617 (1994).

⁹V. V. Aristov, A. I. Erko, and V. V. Martynov, *X-Ray Sci. Technol.* **3**, 211 (1992).

¹⁰A. Sammar and J.-M. André, *J. Opt. Soc. Am. A* **10**, 2324 (1993).

¹¹S. Bac, P. Troussel, A. Sammar, P. Guerin, F.-R. Ladan, J.-M.

- André, D. Schirmann, and R. Barchewitz, *X-Ray Sci. Technol.* **5**, 161 (1995).
- ¹²K. Krastev, F. LeGuern, K. Coat, R. Barchewitz, J.-M. André, M. F. Ravet, E. Cambriel, F. Rousseaux, and P. Davi, *Nucl. Instrum. Methods Phys. Res. A* **368**, 533 (1996).
- ¹³P. Croce and L. Nénot, *Rev. Phys. Appl.* **11**, 113 (1976).
- ¹⁴A. I. Erko, B. Vidal, P. Vincent, Yu. A. Agafonov, V. V. Martynov, D. V. Roschupkin, and M. Brunel, *Nucl. Instrum. Methods Phys. Res. A* **333**, 599 (1993).
- ¹⁵A. S. Davydov, *Quantum Mechanics* (Pergamon, Oxford, 1969).
- ¹⁶E. J. Puik, M. J. Van der Wiel, P. Lambooy, J. Verhoeven, F. E. Christensen, and H. A. Padmore, *X-Ray Sci. Technol.* **3**, 19 (1991).
- ¹⁷L. V. Azaroff, R. Kaplow, N. Kato, R. J. Weiss, A. J. C. Wilson, and R. A. Young, *X-Ray Diffraction* (McGraw-Hill, New York, 1974).
- ¹⁸P. Mikulík, Ph.D. thesis, Université Joseph Fourier (Grenoble) and Masaryk University (Brno), 1997.
- ¹⁹Z. G. Pinsker, *Dynamical Scattering of X-Rays in Crystals* (Springer, Berlin, 1978).
- ²⁰F. Abèles, *Ann. Phys. (Paris)* **127**, 597 (1950).
- ²¹M. Born and E. Wolf, *Principles of Optics* (Pergamon, Oxford, 1993).
- ²²G. T. Baumbach, S. Tixier, U. Pietsch, and V. Holý, *Phys. Rev. B* **51**, 16 848 (1995).
- ²³V. Holý and T. Baumbach, *Phys. Rev. B* **49**, 10 668 (1994).